

## Strong Clustering in the Low Redshift Lyman- $\alpha$ Forest

Andrew Ulmer<sup>1</sup>

Princeton University Observatory, Princeton, NJ 08544-1001

### ABSTRACT

The two-point correlation function,  $\xi$ , of Lyman- $\alpha$  forest is found to be large,  $\xi = 1.8_{-1.2}^{+1.6}$ , > 90% confidence level, on the scale of 250-500 km/s for a sample of absorbers ( $0 < z < 1.3$ ) assembled from HST Key Project Observations. This correlation function is stronger than at high redshift ( $z > 1.7$ ) where  $\xi \approx 0.2$  for velocities  $> 250$  km/s.

*Subject headings:* quasars: absorption lines

### 1. Introduction

Many correlation studies of the Lyman- $\alpha$  forest have been made in the past decades. Almost all of these investigations were limited to redshifts greater than  $\sim 1.7$ , since they were carried out on the ground. After many years of controversial weak detections of the two-point correlation function at  $z > 1.7$  on scales  $< 300$  km/s (Webb 1987, Ostriker, Bajtlik, & Duncan 1988, Rauch et al. 1992, Srianand & Khare 1994, Chernomordik 1995, Cristiani et al. 1995, Kulkarni et al. 1996, Srianand 1996), a consensus may be developing that there is a small, but finite correlation,  $\xi \approx 0.2$  on scales less than 300 km/s (see Cristiani 1995 for a review). In contrast, based on the finding of Cowie et al. (1995), which shows that some high-redshift Ly- $\alpha$  lines have many weak associated carbon lines described as “cloudlets,” Fernández-Soto et al. (1996) report an extremely strong correlation function,  $\xi \approx 10$ , among these weak carbon lines on scales  $\sim 200$  km/s. This finding begs the question of what an individual Ly- $\alpha$  system is. At scales larger than 300 km/s, the correlation at  $z > 1.7$  is to quite weak or undetectable (Sargent et al. 1980, Sargent, Young, & Schneider 1982, Bechtold 1987, Webb & Barcons 1991, Cristiani 1995, Srianand 1996).

---

<sup>1</sup>andrew@astro.princeton.edu

Recently, UV observations with Faint Object Spectrograph of the Hubble Space Telescope have opened up a new regime of redshift space for study,  $z \approx 0-1.3$  (Bahcall et al. 1991, 1992, 1993a (CAT1), 1993b, 1996 (CAT2); Morris et al. 1991). A reasonably strong correlation function among these low-redshift systems might be anticipated because (1) gravitational correlations tend to grow with time, and (2) very low redshift observations of galaxies near quasar lines of sight which show that perhaps one third or more of the Ly- $\alpha$  forest lines are associated with galaxies (Lanzetta et al. 1995; see also Bahcall et al. 1992, Spinrad et al. 1993, Sarajedini, Green, & Jannuzi 1995) which are highly correlated objects. No evidence for a two-point correlation function was found in the first analysis of the Quasar Absorption Line Key Project data (CAT1), although evidence for clumping of the Ly- $\alpha$  forest lines near metal-line systems was discovered (CAT2). Studies of high redshift metal-line systems show strong two-point correlation functions ( $\xi \gtrsim 5$  at 100 km/s) on scales of up to  $\sim 500$  km/s (Sargent, Boksenberg, & Steidel 1988, Heisler, Hogan, & White 1989, Petitjean & Bergeron 1994). Therefore, if the low-redshift Ly- $\alpha$  forest lines are either gravitationally evolved counterparts of high redshift Ly- $\alpha$  lines, are associated with ordinary galaxies, or clump around the strongly clustered metal lines, they should have a relatively strong, yet unmeasured, two-point correlation function.

In this paper, a complete, well-defined sample of low-redshift absorbers is analyzed for a two-point correlation function using techniques that are especially appropriate for quasar absorption lines. In particular, a new algorithm for simulating data with a two-point correlation function allows for a good determination of the errors in the detected correlation function. The paper is organized as follows. In §II, the data are described and the procedure for creating a complete data set is presented. Using extensive Monte Carlo simulations, the two-point correlation function for the Ly- $\alpha$  forest is shown to be non-zero in §III. In §IV, the strength of the two-point correlation is determined, again with use of Monte Carlo simulations. Blends are shown to have only a minimal effect on the findings in §V. A discussion and summary of the results of the paper is given in §VI.

## 2. A Complete Data Set

In order to create a sample free of experimental biases, a subset of Ly- $\alpha$  lines was selected from the published catalogs assembled by the Quasar Absorption Line Key Project from Faint Object Spectrograph (R=1300) observations on the Hubble Space Telescope (CAT1, CAT2). The selection procedure is similar to that described in §VII of CAT2. The Ly- $\alpha$  sample adopted here has a uniform detection limit of  $0.24 \text{ \AA}$ , rest equivalent width, which corresponds to  $\sim 2 \times 10^{14} \text{ HI/cm}^2$  for unsaturated lines. Lines from spectral regions

in which the line detection limit,  $W_{\min}$ , was greater than  $0.24 \text{ \AA}$  are excluded. In other words, no lines are included in the sample which are very weak lines or which come from parts of the spectrum where the sensitivity was low. Because of the proximity effect, lines within 3000 km/s of the quasar emission redshift are excluded.

The total sample consists of 100 Ly- $\alpha$  lines. Nine of these are associated with extensive metal-line systems with four or more detected metal lines (see CAT1, CAT2). The mean redshift of the lines is 0.7.

The complete sample used for analysis in this paper is given in Table 1 and Table 2. The spectral range for each quasar spectrum where the sensitivity was high enough to meet the uniform detection limit criteria is given in Table 3.

### 3. Pairs counts and the Two-point Correlation Function

The two-point correlation function can be estimated from the pair counts in the data according to the formula,

$$\xi(r) = \frac{N(\text{Obs})(r)}{N(\text{Ran})(r)} - 1, \quad (1)$$

where  $N(\text{Obs})$  is the number of observed pairs and  $N(\text{Ran})$  is the number of pairs in a given redshift bin that would be expected in the absence of clustering.  $N(\text{Ran})$  is determined by Monte Carlo simulations. The same velocity bins are used as employed in the first empirical analysis of the two-point correlation function in this data (CAT1).

In the Monte Carlo simulations, the number of pairs expected in the absence of clustering was calculated by placing lines along the part of each quasar line-of-sight where the minimum observable rest equivalent width was less than the uniform detection limit of  $0.24 \text{ \AA}$ . The lines are Poisson distributed with the probability of a line being placed at a given redshift being proportional to the assumed density at the corresponding redshift. Studies of the number density at both high and low redshift have indicated that

$$n(z) \approx A(1+z)^\gamma, \quad (2)$$

where  $n(z)$  is the number density,  $A$  is a normalization constant, and the exponent  $\gamma$  is between 0 and 1.5 in the redshift range of interest (CAT1,CAT2). To mimic the finite resolution of the data in the simulations, lines with separations less than 230 km/s were excluded following CAT1. For each separate data subset investigated, ten thousand simulations were performed which was adequate to fix the error bars reliably. The slope,  $\gamma$ , of the number density was varied between 0 and 1.5, which covers the range allowed by the observational data.

The approach taken here differs from some of the previous analyses of clustering (e.g. CAT1) in two ways. First, the normalization constant,  $A$ , used to produce the number of lines along each line-of-sight, is determined for the entire sample and is the same for every quasar line-of-sight. In previous papers, the Monte Carlo simulations, used to determine  $N(\text{Ran})$  matched the number of simulated lines along the line-of-sight with the observed number of lines along the line-of-sight. The strength of the correlation function will be underestimated if  $A$  is determined, in this way, separately, for each line-of-sight. Monte Carlo simulations show the strength of this normalization effect in this data sample to be about 20% in the sense that the expected number of pairs is decreased by 20% when the normalization done correctly. The effect is most important in data samples with a small number of lines along each line-of-sight where Poisson fluctuations of the number of lines along each line of sight are significant, as is the case for low-redshift studies. Second, the evolution of number density evolution is included in the Poisson distribution. If it were neglected, the number of expected pairs would be underestimated, and the strength of any clustering would be overestimated, because pair counts scale as the square of the density,

$$\Delta N(\text{Ran}) = N(\text{Ran}) \left[ \frac{\int n^2(z) dz}{\int n^2 dz} - 1 \right], \quad (3)$$

where  $n(z)$  is the number density as a function of redshift, and  $n$  is the unevolving number density. In this sample, the strength of this effect is about 20% as well.

Figures 1 and 2 show the pair counts of Ly- $\alpha$  systems alone and for the combined Ly- $\alpha$  and metal-line system subset. For Figure 1, pair separations are calculated in terms of relative velocity as measured by an observer at the absorption systems, and for Figure 2 the separations are shown in terms of comoving coordinates. The relations used to calculate the coordinates are ( $\Omega = 1$ )

$$\Delta v = \frac{c \Delta z}{1 + z}, \quad (4)$$

and

$$\Delta r = \frac{c \Delta z}{H_0(1 + z)^{1.5}}. \quad (5)$$

There do not appear to be any statistically significant differences when the data are analyzed in terms of comoving distance rather than velocity. The slope of the number density affects the expected number of pairs in the absence of clustering,  $N(\text{Ran})$ , and therefore the strength of any correlation. The largest number of expected pairs is found with the largest value of  $\gamma$  (1.5) and the smallest number of expected pairs with  $\gamma = 0$ . The results of the Monte Carlo simulations for ( $\gamma = 0$  and 1.5) are also shown in Figures 1 and 2. The actual slope of the number density is likely between these values, and correspondingly, the true  $N(\text{Ran})$  lies between the values resulting from these Monte Carlo simulations.

For both samples and separation measures, there is a strong excess of pairs in the first bin corresponding to 250-500 km/s or 2.5-5  $h^{-1}$ Mpc. Table 4 shows the results of the Monte Carlo experiments that were designed to determine the statistical significance of the observed correlation. The probability that an unclustered distribution could produce in the first bin an excess as high as observed is less than 0.5% in all the cases considered. The probabilities reported in Table 4 are conservative in the sense that,  $\gamma$ , was taken to be 1.5 which is as large as allowed by observation at  $2\sigma$ , so that  $N(\text{Ran})$  was as large as possible.

#### 4. Strength of the Correlation Function

The allowed range of strength of the two point correlation function is determined by Monte Carlo simulations (see Table 4). Because the correlation function is detected in only the first bin of the pair counts, the shape of the correlation function was taken as a free parameter. As shown below, this freedom does not strongly affect the range of the determined strength.

To test the strength of the observed correlation function by Monte Carlo simulation, an algorithm was devised to create a one-dimensional sample with a specified two point correlation function. The many 3-dimensional methods for generating correlated sets of objects (e.g. Neyman, & Scott 1952, Soneira & Peebles 1977) diverge in 1-dimension. Therefore, a different algorithm was developed for the 1-dimensional application in this paper. Details of the algorithm and its relation to 3-D methods will be described in detail in a future paper (Ulmer 1996); a brief description is supplied in Appendix A.

Confidence regions were established by determining what the strongest (weakest) simulated correlation function for which X% of the simulations had as few (as many) pairs in the first bin as the data. Evolution of the number density (Eq. 2) has an effect on the expected number of pairs in the absence of clustering, and therefore on the strength of the correlation function (see Figures 1 and 2). Table 4 lists the minimum,  $\xi_{\min}$ , and the maximum,  $\xi_{\max}$ , values of the correlation function evaluated at the 90% confidence limits in the 250-500 km/s bin. The value of  $\xi_{\min}$  ( $\xi_{\max}$ ) was established by requiring that less than 5 functions smaller (larger) than the value found in the actual sample. The confidence regions given in Table 4 account for this uncertainty in a conservative fashion. For instance, the upper limit of the confidence region,  $\xi_{\max}$ , is found using simulations with the smallest allowable number density slope,  $\gamma = 0$ , which implies the smallest number of expected pairs, and therefore the largest correlation function. Then,  $\xi_{\max}$ , is equal to the value of the correlation function, evaluated in the 250-500 km/s bin, which has the number of pairs in the first bin larger than those observed in 95% of the trials.

In principle, the confidence regions will depend on all n-point correlation functions, or equivalently, the exact algorithm used to create the simulation. In this particular case where the pair counts in only one bin are examined, the 90% confidence regions given in Table 4 is not expected to be too sensitive to the particular type of correlation function used in the simulated data. To test this hypothesis, a variety of two-point and three-point correlation functions were simulated and thereby used to construct confidence intervals. The intervals derived were found to be consistent with those reported in Table 4 to within 5% of their values. Specifically, confidence regions were determined from simulated data with two-point correlation functions of the form which describes galaxies and clusters (Peebles 1980)

$$\begin{aligned} \xi(r) &= -1; & (r < r_{\min}) \\ \xi(r) &= (r/r_0)^{-\gamma}; & (r > r_{\min}) \end{aligned} \tag{6}$$

with  $r_{\min}$  corresponding to the resolution of the data and the exponent,  $\gamma$ , ranging between 1.3 and 2.3. A particular type of three-point correlation function which is appropriate for galaxies was also added with a strength parameter  $Q$  ranging from 0.5-1 (Peebles 1980). While the Ly- $\alpha$  forest may not have the same two and three point correlation functions as described above, the important point is that the confidence regions of the strength of the correlation function are insensitive to the specific shape of correlation function.

The top panel of Figure 3 illustrates the confidence intervals for one of the cases in Table 4. For comparison, the galaxy-galaxy correlation function is shown in the bottom panel of the figure. The galaxy-galaxy correlation function is within the confidence limits determined by Monte Carlo simulations.

## 5. Influence of Blends

In this section, the reality of the close pairs and the possible influence of blends on the observed pairs is investigated. Table 5 gives detailed information about each pair in the 250-500 km/s bin which shows the excess. The average and median equivalent widths of the lines in the close pairs are indistinguishable from that of the entire sample.

In the absence of clustering, the low number density of Ly- $\alpha$  lines at small redshift makes blending much less of a problem than at larger redshifts. The resolution of the Faint Object Spectrograph is 1300 (CAT1) which corresponds to 230 km/s. Then, the number of expected blended lines, that is, lines with separations less than 230 km/s, in the entire sample is  $\sim 4$ . If the blended lines were separated by the line selection algorithm into pairs of lines with separations greater than 250 km/s, an artificial excess of close pairs could be created in the sense that the 250-500 km/s bin would contain all pairs with

actual separations between 0 and 500 km/s. This contamination is unlikely to contribute strongly to the excess detected pairs, because such artificial pairs should have separations just larger than the resolution limit, whereas the close pairs shown in Table 5 do not show this property.

A single line convolved with the instrumental profile and sufficient noise may, in principle, be artificially split into a pair by the automated line selection algorithm. The efficiency of such splittings can be assessed by Monte Carlo experiments using the detailed simulation software developed by the QSO absorption Key Project team (Schneider et al. 1993). D. Schneider (private communication, 1996) generously ran 6000 lines through the Key Project line-simulation software which adds noise, accounts for instrumental resolution, and implements the same line selection routine that was used on the actual Hubble data. The results are very encouraging. Even, if all 100 lines in the sample had a huge internal velocity dispersion of 300 km/s (typical velocity dispersions are 15-50 km/s at  $z \sim 2$ , e.g. Kulkarni et al. 1996), and a large rest equivalent width of 0.67 as did the first 3000 simulated lines (the actual lines are distributed as an exponential distribution with scale  $\sim 0.32 \text{ \AA}$ ), the estimated total number of lines expected to be artificially split into lines with separation greater than 250 km/s in the entire data set is only 0.56. The actual number of artificial pairs in the data is probably much smaller. First, many of the lines in the sample are so weak that even they could not be split into two lines which would exceed the uniform detection limit of  $0.24 \text{ \AA}$ , rest equivalent width. The effective cutoff in rest equivalent width for a line to be able to split into two lines in the sample occurs above  $2 \times 0.24 = 0.48 \text{ \AA}$ , and is closer to  $0.6 \text{ \AA}$ , because lines do not often split exactly into equal parts. The fraction of lines in the sample with rest equivalent width  $> 0.6 \text{ \AA}$  is  $\sim 0.3$ , so the total number of expected artificial pairs is reduced to  $\sim 0.17$ . Further, most Ly- $\alpha$  lines probably have velocity dispersions much less than 300 km/s, and are therefore less likely to split into artificial pairs. We conclude that the effect of blends is no more than 5% on the total number of detected pairs and probably substantially less. Even in the pathological case that all lines had gigantic velocity dispersions of 500 km/s which was the case for the second set of 3000 simulated lines, simulations and the same line of argument shows that the total number of artificial pairs is expected to be less than 0.7. This pathological case would affect slightly the confidence regions described in the previous section, but would still not account for all of the excess close pairs.

Because the close pairs are real, the Ly- $\alpha$  lines are strongly clustered. This clustering will effect the number of blends in the medium resolution data and has important implications for further analyses of the Ly- $\alpha$  forest in this medium resolution data set. For instance, correlations affect the answer to the question: if the data could be viewed under higher resolution, would many of the lines be resolved into multiple systems? Under

the hypothesis that all lines are unclustered, one expects only about 4 (of 100) lines to be composed of two smaller lines (by random superpositions), because of the extremely low line-of-sight density of absorbers. The difference in inferred volumed density of Ly- $\alpha$  absorbers would be only  $\sim 4\%$  as obtained from high and low resolution observations. However, the lines appear to be strongly correlated, and the number of expected unresolved pairs (with  $\Delta v < 230$  km/s) is at least as large the total number of resolved pairs with  $230 \text{ km/s} < \Delta v < 460 \text{ km/s}$  – about 10. If the correlation function increases for velocities less than 250 km/s, as may be the case for high redshift, higher resolution studies, then the number of unresolved pairs may be more than twice as large, or 20 (this would be the case, for instance, if the shape of the correlation function were a Gaussian with zero mean and scale  $\sim 250$ km/s). In the absence of clustering, resolution is expected to make a very small difference in the determination of the statistics of the Ly- $\alpha$  forest, e.g. the number density and number density evolution. Viewed under high resolution and with strong clustering, the number density and evolution of Ly- $\alpha$  forest may easily differ by factors of  $\sim 20\%$  from their presently determined values.

## 6. Discussion and Conclusion

The two-point correlation function,  $\xi$ , of Ly- $\alpha$  forest lines,  $\langle z \rangle = 0.7$ , is  $\xi = 1.8_{-1.2}^{+1.6}$ , 90% confidence level, for separations of 250-500 km/s (see Table 4).

How does the clustering at low redshifts compare with the recent detections of high redshift clustering? Between redshifts of 1.7 and 4, for similar velocity separations and equivalent width limits, it seems likely that the correlation function is  $\lesssim 0.2$  on scales greater than 250 km/s (see Cristiani 1995 and references therein; see Fernández-Soto et al. 1996 for a different view). Additionally, Cristiani’s investigation shows some evidence for the increase of the correlation function (for velocity separations of 100 km/s) with decreasing redshift. Similar findings have also been reported by Srianand (1996).

In velocity space, the correlation function has strengthened with redshift from  $\xi \lesssim 0.2$  at high redshifts to  $\xi \gtrsim 1$  at the small redshifts considered. The interpretation of the increasing correlation function is not straightforward. For instance, the low and high redshift absorbers may not be the same (see the discussion in CAT2 and references therein).

How does the detected strength of the Ly- $\alpha$  correlation function compare to that of galaxies? Such a comparison is motivated in part by the long-standing idea that Ly- $\alpha$  absorbers are related to the halos of galaxies (e.g. Bahcall 1979, Mo 1994) as well as by the finding that at very low redshift, perhaps one third or more of the Ly- $\alpha$  lines are associated

with galaxies (Lanzetta et al. 1995). A zeroth-order comparison is made in the second panel of Figure 3 by plotting the galaxy-galaxy correlation function ( $z = 0$ ) against the observed Ly- $\alpha$  correlation function. The two correlation functions are consistent within the limits of the data. Even the simplest galactic-halo Ly- $\alpha$  forest models have as many as 4 free parameters: velocity dispersion of galaxies as a function of redshift, evolution of the galaxy-galaxy correlation function, fraction of galaxies with Ly- $\alpha$  lines, and the truncation point of the spatial two-point correlation function. Therefore, a detailed analysis of the idea that galactic halos and Ly- $\alpha$  lines are related will have to wait until greater amounts of data are collected and good estimates of both the amplitude and the shape of the correlation function become available.

AU is supported by a NSF Graduate Research Fellowship. I thank J. N. Bahcall, J. Miralda-Escude, and H. J. Mo for stimulating and informative discussions, and D. P. Schneider for helping to investigate the possibility of false line pairs in the observations.

## 7. Appendix A

In this appendix, the algorithm for simulating data with a given two-point correlation function is briefly described. A further description as well as sample code for implementing the algorithm will be provided elsewhere (Ulmer 1996). It was necessary to devise a new algorithm, because traditional 3-dimensional algorithms (e.g. Neyman, & Scott 1952, Soneira & Peebles 1977) diverge in 1-dimension.

The algorithm generates a 1-dimensional set of points with two-point correlation functions of the form

$$\begin{aligned} \xi(r) &= -1; & (r < r_{\min}) \\ \xi(r) &= (r/r_0)^{-\gamma}; & (r > r_{\min}) \end{aligned} \tag{7}$$

There are three free parameters in the correlation function:  $\gamma$ ,  $r_0$  and  $r_{\min}$ .

The algorithm can be motivated by writing the conditional probability of finding one object in the element  $dr$  at a distance  $\Delta r$  from another object,

$$dP = n(1 + \xi(\Delta r))dr, \tag{8}$$

where  $n$  is the density. A first approach to generating a 1-dimensional data set with a two-point correlation function could be to (1) start with an object at  $r = 0$  and (2) place a second object at  $r_1 = \Delta r_1$  according to a Poisson process with probability of an object being placed at  $\Delta r$  ( $> 0$ ) as determined by Eq. 8, (3) place the third object at  $r_2 = r_1 + \Delta r_2$  according to Eq. 8, that is place the object only with reference to the one directly preceding it (4) place the  $i$ th object at  $r_i = r_{i-1} + \Delta r_i$ , and so on. The simulated data produced by this algorithm has some flaws. First, the density of the simulated data is not necessarily  $n$ , because the probability of placing an object is smaller than  $n dr$  when  $r < r_{\min}$  and greater than  $n dr$  when  $r > r_{\min}$ , and they need not cancel out. Second, the slope and scale of the two-point correlation in the simulated data are not exactly the same as specified by the input parameters,  $\gamma$ ,  $r_0$  and  $r_{\min}$ .

These problems can be solved by using a slightly different correlation function  $\tilde{\xi}$  with an extra parameter,  $\epsilon$ , that can be tuned so that the algorithm produces the correct density. We write this correlation function as

$$\begin{aligned} \tilde{\xi}(r) &= -1; & (r < r_{\min}^{\tilde{}}) \\ \tilde{\xi}(r) &= (r/\tilde{r}_0)^{-\tilde{\gamma}} - \epsilon; & (r > r_{\min}^{\tilde{}}), \end{aligned} \tag{9}$$

where  $\epsilon$  is between 0 and 1. The other input parameters,  $\tilde{\gamma}$ ,  $\tilde{r}_0$  and  $r_{\min}^{\tilde{}}$ , differ slightly from  $\gamma$ ,  $r_0$  and  $r_{\min}$ . The final algorithm is therefore identical to the one given above except that the probability of finding a point at a given separation,  $\Delta r$  from another is given by

$$dP = n(1 + \tilde{\xi}(\Delta r))dr \tag{10}$$

The algorithm is able to produce data with the desired two-point correlation function with high accuracy to over 10 scale lengths in radius for the densities and correlations appropriate for this study.

## REFERENCES

- Bahcall, J.N. 1979, in Longair, M.S. & Warner, J.N. eds., Proc of IAU Coll 54 on “Scientific Research with the Space Telescope,” NAS CP-2111, p. 215
- Bahcall, J. N., et al. , 1993a, ApJS., 87, 1 (CAT1)
- Bahcall, J. N., et al. , 1996, ApJ., 457, 19 (CAT2)
- Bahcall, J.N., Jannuzi, B.T., Schneider, D.P., Hartig, G.F., Bohlin, R., & Hunkkarinen, V. 1991, ApJ, 377, L5
- Bahcall, J. N., Jannuzi, B.T., Schneider, D.P., Hartig, G.F., & Green, R.F. 1992, ApJ, 397, 68
- Bahcall, J. N., Jannuzi, B.T., Schneider, D.P., & Hartig, G.F., 1993b, ApJ, 405, 491
- Bechtold, J., 1987 in Bergeron, J. et al. eds., Proc. Third IAP Workshop, High Redshift and Primeval Galaxies, Editions Frontieres, Gif-sur-Yvette, p. 397
- Chernomordik, V.V., 1995, ApJ 440, 431
- Cowie, L.L., Songaila, A., Kim, T.-S., & Hu, E.M., 1995, AJ, 109 1522
- Cristiani, S. 1995, preprint, astro-ph/9512086 and ESO preprint 1117
- Cristiani, S., D’Odorico, S., Fontana, A., Giallongo, E., Savaglio, S., 1995 MNRAS 273, 1016
- Fernández-Soto, A., Lanzetta, L.M., Barcons, X., Carswell, R.F., Webb, J.K., Yahil, A. 1996, ApJ, 460, L85
- Heisler, J., Hogan, C. J., & White, S. D. M., 1989, ApJ, 347, 52
- Kulkarni, V.P., Huang, K., Green, R.F., Bechtold, J., Welty, D.E., & York, D.G. 1996, MNRAS *in press*
- Lanzetta, K. M., Bowen, D. V., Tytler, D., & Webb, J. K. 1995, ApJ, 442, 538
- Mo, H.J., 1994, MNRAS 269, P49
- Neyman, J. & Scott, E.L. 1952, ApJ 116, 144
- Ostriker, J.P., Bajtlik, S., & Duncan, R.C. 1988, ApJ, 327, L35

- Peebles, P.J.E., 1980, *The Large Scale Structure of the Universe*, Princeton University Press, Princeton, NJ
- Petitjean, P & Bergeron, J., 1994, *A&A*, 283, 759
- Rauch, M. & et al. 1992, *ApJ* 390, 387
- Sarajedini, V.L., Green, R.F., & Jannuzi, B.T. 1995, preprint astro-ph/9508068
- Sargent, W.L.W., Boksenberg, A., Steidel, C.C., 1988, *ApJS* 68, 539
- Sargent, W. L. W., Young, P. J., Boksenberg, A., & Tytler, D. 1980, *ApJS*, 42, 41
- Sargent, W. L. W., Young, P. J., Schneider, D.P. 1982, *ApJ*, 256, 374
- Schneider,D.P. et al. 1993, *ApJS*, 87, 45
- Schneider,D.P. 1996, private communication
- Soneira, R.M. & Peebles, P.J.E. 1977, *ApJ*, 211,1
- Sprinrad, H. et al. 1993, *AJ* 106, 1
- Srianand, R. 1996, *ApJ*, Submitted.
- Srianand, R. & Khare, P. 1994, *MNRAS*, 271, 81
- Ulmer, 1996, in preparation
- Webb, J.K., 1987, in Hewett, A., Burbidge, G., Fang, L.Z. eds., *Proc. IAU Symp. 124, Observational Cosmology*, Reidel, Dordrecht, p. 803
- Webb, J.K. & Barcons, X. 1991, *MNRAS* 250, 270

Table 1: Lyman-alpha lines in sample from the first HST Key Project catalog (CAT1). Daggers ( $\dagger$ ) denote extensive metal-line systems. Equivalent widths are given in the rest frame. All values are given in Angstroms.

$\lambda_{\text{obs}}$	EqW	Object	$\lambda_{\text{obs}}$	EqW	Object	$\lambda_{\text{obs}}$	EqW	Object
1743.3	0.33	3C 95	1486.6	0.34	3C 351	2046.0	0.43	PKS 2145+06
1750.2	0.49	3C 95	1535.0	0.30	3C 351	2104.1	0.49	PKS 2145+06
1910.6	0.47	3C 95	1561.5	0.62	3C 351	2165.1	0.69	PKS 2145+06
1959.9	0.40	3C 263	1563.9	0.37	3C 351	2177.6 $\dagger$	1.22	PKS 2145+06
1980.7	0.35	3C 263	1363.5	0.53	H 1821+643	2210.1	0.25	PKS 2145+06
1296.5	0.30	3C 273	1365.4	0.32	H 1821+643	2247.7	0.55	PKS 2145+06
1482.7	0.54	PG 1259+593	1394.1	0.58	H 1821+643	2258.3	0.38	PKS 2145+06
1487.2	0.25	PG 1259+593	1422.8	0.64	H 1821+643	2285.1	0.71	PKS 2145+06
1571.6	0.34	PG 1259+593	1435.2	0.30	H 1821+643	2082.6	0.27	3C 454.3
1411.5	0.29	3C 351	1475.4	0.46	H 1821+643	2118.1	0.59	3C 454.3
1444.2	0.36	3C 351	1489.4	0.75	H 1821+643	2211.6	0.33	3C 454.3
1485.0 $\dagger$	0.93	3C 351	1576.9 $\dagger$	0.52	H 1821+643	2215.6	0.47	3C 454.3

Table 2: Lyman-alpha lines in sample from the second HST Key Project catalog (CAT2). Daggers (<sup>†</sup>) denote extensive metal-line systems. Equivalent widths are given in the rest frame. All values are given in Angstroms.

$\lambda_{\text{obs}}$	EqW	Object	$\lambda_{\text{obs}}$	EqW	Object	$\lambda_{\text{obs}}$	EqW	Object
1866.0	0.29	TON 153	2276.6	0.40	PKS 0122-00	2332.4	0.32	PG 1634+706
1949.9	0.32	TON 153	2303.5	0.70	PKS 0122-00	2342.3	0.46	PG 1634+706
1983.1	0.45	TON 153	1843.0	0.28	PG 1352+011	2388.7	0.77	PG 1634+706
2018.8 <sup>†</sup>	1.48	TON 153	1846.5	0.45	PG 1352+011	2412.0	0.45	PG 1634+706
2029.2	0.60	TON 153	1849.0	0.25	PG 1352+011	2416.8	0.25	PG 1634+706
2032.1	0.39	TON 153	1852.0	0.41	PG 1352+011	2420.1 <sup>†</sup>	1.10	PG 1634+706
2034.5	0.78	TON 153	1855.1 <sup>†</sup>	2.62	PG 1352+011	2435.9	0.60	PG 1634+706
2036.9	0.78	TON 153	1894.3	0.37	PG 1352+011	2453.0	0.51	PG 1634+706
2038.8	0.27	TON 153	1941.7	0.39	PG 1352+011	2481.6 <sup>†</sup>	1.42	PG 1634+706
2060.9	0.73	TON 153	1946.7	0.76	PG 1352+011	2501.4	0.46	PG 1634+706
2107.9	0.54	TON 153	1989.6	0.48	PG 1352+011	2538.5	0.62	PG 1634+706
2118.1	0.26	TON 153	2019.0	0.52	PG 1352+011	2560.9	0.37	PG 1634+706
2159.4	0.41	TON 153	2022.1	0.34	PG 1352+011	2564.9	0.28	PG 1634+706
2178.0	0.29	TON 153	2027.6 <sup>†</sup>	0.94	PG 1352+011	2599.9	0.90	PG 1634+706
2223.9	0.25	TON 153	2062.3	0.48	PG 1352+011	2603.3	0.48	PG 1634+706
2244.5	0.30	TON 153	2107.2	0.43	PG 1352+011	2628.7	0.24	PG 1634+706
2254.5	0.43	TON 153	2150.8	0.44	PG 1352+011	2672.0	0.31	PG 1634+706
2276.4	0.42	TON 153	2188.2	0.28	PG 1352+011	2677.4	0.25	PG 1634+706
2077.9	0.82	PKS 0122-00	2212.0	0.32	PG 1352+011	2706.9	0.47	PG 1634+706
2098.8	0.28	PKS 0122-00	2224.5	0.25	PG 1352+011	2778.1	0.25	PG 1634+706
2226.9	0.47	PKS 0122-00	2317.2 <sup>†</sup>	0.49	PG 1634+706			
2265.7	0.58	PKS 0122-00	2324.5	0.67	PG 1634+706			

Table 3: Coverage of each observed quasar spectrum (CAT1, CAT2) in which the sensitivity to meet the uniform detection limit of  $0.24 \text{ \AA}$  described in §2 is achieved. Wavelengths are given in Angstroms.

$\lambda_1$	$\lambda_2$	Object
-	-	PG 0043+039
1906	1953	PKS 0044+03
1728	1941	3C 95
1795	1820	US 1867
1903	1987	3C 263
1235	1393	3C 273
1335	1600	PG 1259+593
1641	1648	B2 1512+37
1332	1600	3C 351
1319	1600	H 1821+643
2022	2307	PKS 2145+06
2032	2307	3C 454.3
-	-	PKS 2251+11
1733	2307	TON 153
2030	2307	PKS 0122-00
1767	2307	PG 1352+011
2260	2807	PG 1634+706

Table 4: Probability of observed excess in first bin as determined from Monte Carlo simulations. The strength of the correlation function on the scale of 250-500 km/s,  $\xi$ , is large. The 90% confidence intervals,  $\xi_{\min}$  and  $\xi_{\max}$ , are determined by Monte Carlo simulations as described in § IV. They are conservative intervals in that they are slightly  $> 90\%$  confidence intervals.

Prob	Metal lines	$\Delta v$ or $\Delta r$	$\xi$	$\xi_{\min}$	$\xi_{\max}$
0.0047	no	$\Delta v$	1.8	0.6	3.4
0.0011	yes	$\Delta v$	2.1	0.9	3.5
0.0013	no	$\Delta r$	2.0	0.9	3.7
0.0004	yes	$\Delta r$	2.2	1.0	3.5

Table 5: Ly- $\alpha$  line pairs in the range 250-500 km/s. Pairs with a dagger ( $\dagger$ ) are those pairs which include a metal-line system. Equivalent widths are given in rest frame coordinates. All values are given in Angstroms.

$\lambda$	$\Delta\lambda$	EqW <sub>1</sub>	EqW <sub>2</sub>	Object
1485.8 $\dagger$	1.6	0.92	0.34	3C 351
1562.7	2.4	0.62	0.37	3C 351
1364.4	2.0	0.32	0.53	H 1821+643
2030.6	2.9	0.60	0.40	TON 153
2033.3	2.4	0.39	0.78	TON 153
2035.7	2.5	0.78	0.78	TON 153
2037.9	1.8	0.78	0.27	TON 153
1847.8	2.4	0.45	0.25	PG 1352+011
1850.5	3.0	0.25	0.41	PG 1352+011
1853.5 $\dagger$	3.1	0.41	2.62	PG 1352+011
2020.5	3.1	0.52	0.34	PG 1352+011
2418.5 $\dagger$	3.3	0.25	1.10	PG 1634+706
2562.9	4.0	0.37	0.28	PG 1634+706
2601.6	3.5	0.90	0.48	PG 1634+706

Fig. 1.— Observed number of pairs as a function of velocity separation (solid lines) show a strong excess at the smallest velocity scales. The expected number of pairs in absence of clustering (dashed lines) are given for two values of the number density evolution,  $\gamma = 0$  and 1.5 as determined from extensive Monte Carlo simulations. In the top panel, metal-line systems are excluded from the sample.

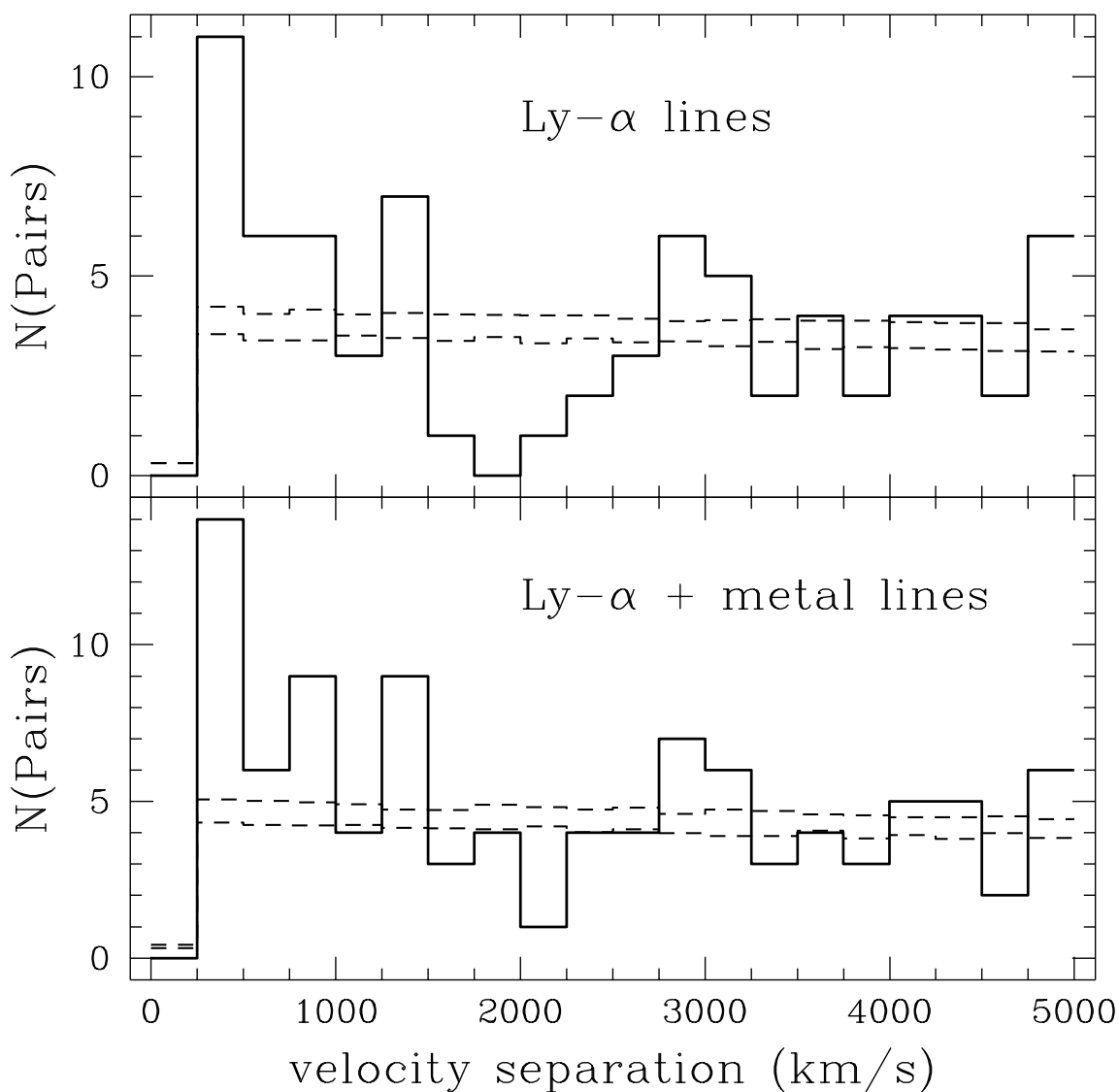


Fig. 2.— Same as Figure 1, except the number of pairs are measured as a function of comoving separation assuming no peculiar velocities for the absorbers.

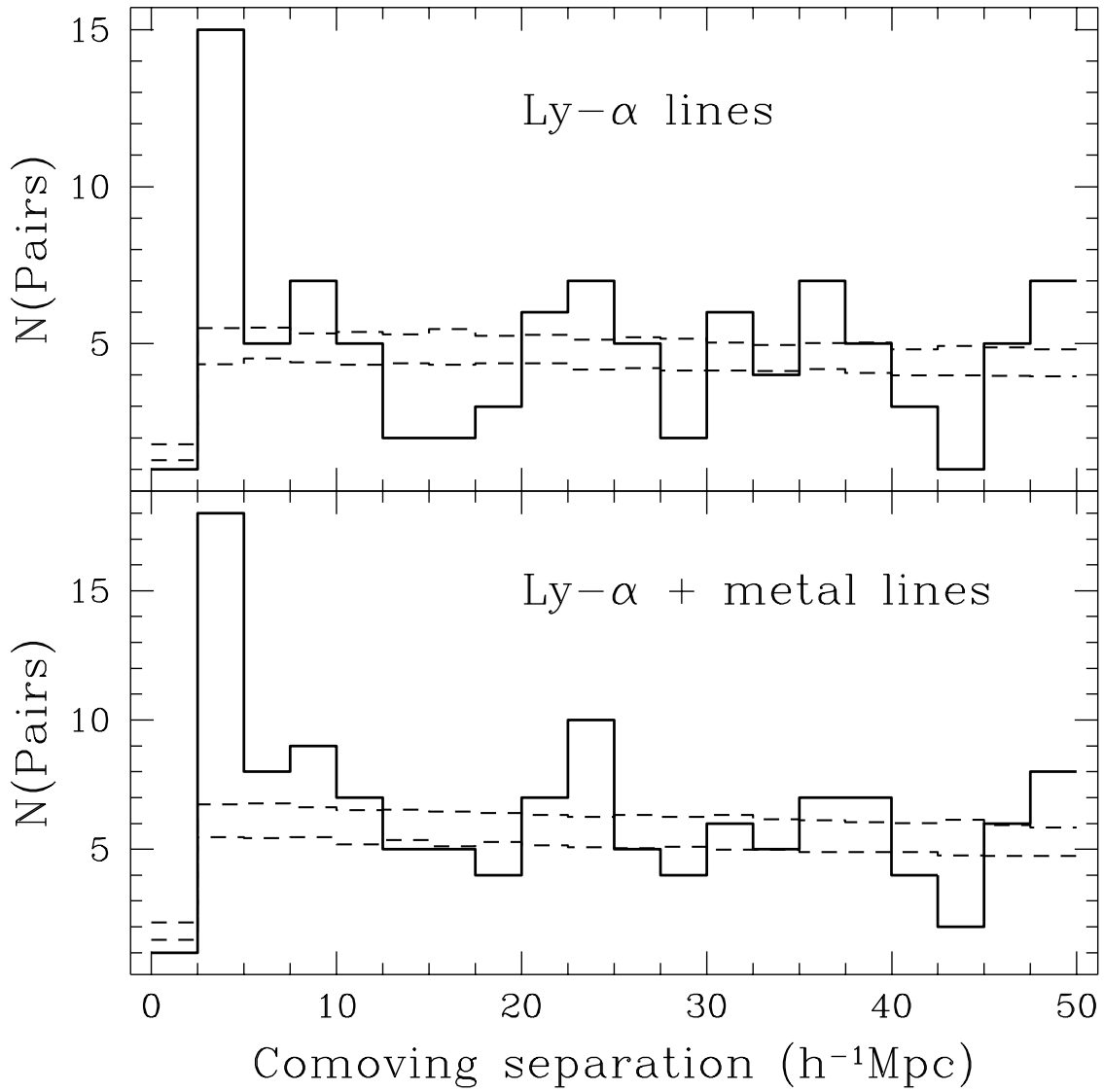


Fig. 3.— The top panel shows the observed number of pairs (solid line) for the Ly- $\alpha$  lines (with metal lines excluded). The upper and lower confidence intervals as determined by Monte Carlo experiments are indicated with dashed lines. As described in §4, confidence limits apply to the first bin alone. The bottom panel shows the same observed number of pairs (solid line) as in the top panel with the galaxy-galaxy correlation function ( $z = 0$ ) shown as a dashed line. The two functions are similar in strength; however, the absorbers likely have peculiar velocities, so the two correlation functions are not directly comparable.

